

1 **Effects of rhamnolipid and carboxymethylcellulose**
2 **coatings on reactivity of palladium-doped nanoscale**
3 **zerovalent iron particles**

4
5
6
7 Sourjya Bhattacharjee¹, Mohan Basnet², Nathalie Tufenkji², Subhasis Ghoshal^{1,*}

8 ¹Department of Civil Engineering, McGill University, Montreal, QC H3A 0C3, Canada

9
10 ²Department of Chemical Engineering, McGill University, Montreal, QC H3A 0C5, Canada

11
12 **Environmental Science and Technology**

13 January 5, 2016

14
15
16
17
18
19
20 *Corresponding author phone: 514-398-6867; fax: 514-398-7361; email: subhasis.ghoshal@mcgill.ca

ABSTRACT

Nanoscale zerovalent iron (NZVI) particles are often coated with polymeric surface modifiers for improved colloidal stability and transport during remediation of contaminated aquifers. Doping the NZVI surface with palladium (Pd-NZVI) increases its reactivity to pollutants such as trichloroethylene (TCE). In this study, we investigate the effects of coating Pd-NZVI with two surface modifiers of very different molecular size: rhamnolipid (RL, anionic biosurfactant, M.W. 600 g mol⁻¹) and carboxymethylcellulose (CMC, anionic polyelectrolyte, M.W. 700000 g mol⁻¹) on TCE degradation. RL loadings of 13 to 133 mg TOC/g NZVI inhibited deposition of Pd in a concentration-dependent manner, thus limiting the number of available Pd sites and decreasing the TCE degradation reaction rate constant from 0.191 h⁻¹ to 0.027 h⁻¹. Furthermore, the presence of RL in solution had an additional inhibitory effect on the reactivity of Pd-NZVI by interacting with the exposed Pd deposits after they were formed. In contrast, CMC had no effect on reactivity at loadings up to 167 mg TOC/g NZVI. There was a lack of correlation between Pd-NZVI aggregate sizes and TCE reaction rates, and is explained by cryo-transmission electron microscopy images that show open, porous aggregate structures where TCE would be able to easily access Pd sites.

INTRODUCTION

Nanoscale zerovalent iron (NZVI) has generated considerable interest for environmental remediation because it can rapidly transform a variety of heavy metal and chlorinated organic contaminants through chemical reduction processes.¹ However, there are challenges associated with efficient utilization of NZVI particles, which include the loss of electrons due to reaction with water² and the passivation of NZVI surface due to formation of oxide layers³, leading to reduced reactivity towards target contaminants. Furthermore, the attractive magnetic forces that exist between NZVI particles lead to significant aggregation and pose a challenge to their transport in contaminated aquifers during *in situ* remediation.⁴⁻⁶ In order to mitigate problems associated with aggregation and stability, NZVI is often coated with surface modifiers such as polyelectrolytes and surfactants to increase the efficiency of their transport in the subsurface.⁶⁻¹²

Doping the NZVI surface with palladium (Pd-NZVI) enhances contaminant degradation rates by orders of magnitude compared to bare NZVI particles, and addresses the challenges of the loss of electrons to reactions with water.¹³⁻¹⁷ Typically such rate enhancements are facilitated through the rapid conduction of electrons between the Fe⁰ core and the contaminant via a galvanic couple formation between Fe⁰ and Pd⁰, and/or through the role of Pd⁰ as a hydrogenation catalyst.¹⁸ In the latter process, the rapid degradation of target chlorinated contaminants is facilitated by atomic hydrogen species generated by Pd⁰, from H₂ generated by the reduction of H₂O by Pd-NZVI. A few studies^{7, 8, 14, 19-21} have investigated the reactivity of Pd-NZVI coated with surface modifier polymers or surfactants because *in situ* remediation applications of Pd-NZVI will require colloidal stabilization of the particles, and thus understanding the role of surface modifiers on reactivity is important.

A number of different types of surface modifiers have been used in the literature to coat NZVI and Pd-NZVI particles ranging from longer chain polyelectrolytes such as polyvinylpyrrolidone (PVP) and CMC^{8, 14}, to shorter chain surfactants such as rhamnolipid (RL)⁹. He and Zhao¹⁹ synthesized CMC-coated Pd-NZVI with various CMC loadings and observed that the trichloroethene (TCE) degradation rate of the nanoparticles increased with CMC loadings up to an optimum CMC to Fe ratio of 0.0124 and attributed the increase to smaller particle sizes generated by the increasing CMC dose. However, the authors noted that the increase in the degradation rate was not directly proportional to increases in specific surface area. At CMC concentrations higher than the optimum, the TCE degradation rate decreased, and this decrease was attributed to the unavailability of reactive sites caused by adsorption of CMC. Sakulchaicharoen et al.¹⁴ investigated the effects of CMC, PVP (360K and 40K) and guar gum on Pd-NZVI reactivity. The authors reported that some stabilizers such as CMC increased the TCE degradation by an order of magnitude compared to non-stabilized

Pd-NZVI while other stabilizers such as PVP 40 K and guar gum reduced the TCE degradation rate. The increase in reactivity was attributed to smaller particle sizes of Pd-NZVI while the decrease in reactivity was attributed to reactive site inaccessibility by TCE. In all of these studies, surface modifiers were pre-grafted to the particle. NZVI particles can be coated with surface modifiers either by post-grafting or pre-grafting¹⁰. For pre-grafting, Fe salt solutions are first mixed with surface modifiers and then chemically reduced to obtain the surface modifier-coated NZVI particle. For post-grafting, surface modifiers are mixed with bare NZVI particles and allowed to adsorb onto the nanoparticle surface. Once the surface modifier-coated NZVI particles are synthesized through either approach, Pd salts are added to the nanoparticles and Pd⁰ deposits are formed on the surface of NZVI yielding the surface modifier coated Pd-NZVI particles. In this study, as well as in other studies^{8, 14, 19, 21}, Pd is added as the last step in the synthesis and after equilibration of NZVI with the surface modifier, to avoid rapid loss of substantial amounts of Fe(0) in reaction with water, before commencement of the TCE reactivity assessment.

A few studies provide insights on the impacts of surface modifier on the reactivity of non-palladized NZVI. Phenrat et al.²² reported a decrease in TCE degradation rate constants for NZVI particles post-grafted with 3 different polyelectrolytes, namely polystyrene sulfonate, CMC and polyaspartate. The authors cited blockage of surface reactive sites and decrease in availability of aqueous TCE at the NZVI surface due to displacement of the aqueous phase by the adsorbed polymer layers as reasons for decreased reactivity. Sun et al.²³ employed polyvinyl alcohol-co-vinyl acetate-co-itaconic acid (PV3A) in a pre-grafting approach to coat non-palladized NZVI particles and observed that uncoated NZVI and PV3A coated NZVI had similar TCE degradation rates although their mean diameters were 100 and 15 nm, respectively. The authors attributed the similarity in degradation rates of coated and uncoated NZVI particles to equal availability of reactive surface areas. Although PV3A-NZVI were smaller with a higher surface area, it was proposed that a large fraction of its reactive surface was occupied by the adsorbed PV3A molecules and unavailable for direct reaction with TCE.

Zhu et al.²⁴ reported that the presence of surfactants (SDS, NPE and CTAB) in solution at low concentrations (below critical micelle concentration) nearly doubled the degradation rate of 1,2,4-TCB by Pd-NZVI. The authors suggested that the surfactants adsorbed to the Pd-NZVI and thereby enhanced the accumulation of the contaminant at the Pd-NZVI surface. The authors noted that at higher concentrations of surfactants in solution, contaminant degradation rates by Pd-NZVI were lower, and speculated that it was likely due to the blocking of the Pd sites.

The above studies suggest that the mass of surface modifiers associated with Pd-NZVI or NZVI may influence its reactivity either positively or negatively. Because the Pd deposits are considered as the primary reaction

sites on Pd-NZVI particles¹⁸, the influence of the surface modifiers on the Pd deposition and binding of the surface modifiers to the Pd deposits would largely affect the reactivity. However, studies to date have not examined whether the surface modifiers sorb on the NZVI surface (exclusive of the Pd sites) or if sorption to Pd deposits on the surface influence the reactivity. The objective of this study was to assess the effects of sorbed surface modifier concentrations on Pd deposition efficiency and TCE degradation rates for Pd-NZVI particles post-grafted with two different surface modifiers, CMC and RL.

CMC (M.W. 700000 g mol⁻¹) is a non-toxic and biodegradable anionic polyelectrolyte and RL (average M.W. 600 g mol⁻¹) is an anioinic biosurfactant. Further details on the surface modifiers used are provided in Table S1. These surface modifiers have been shown to significantly improve transport (reduce deposition and retention) of Pd-NZVI or NZVI in a variety of groundwater compositions and granular materials in our prior studies.^{9, 10, 25-27} However, there are no reports in literature on how post-grafting Pd-NZVI with CMC or biosurfactants such as RL affects its reactivity. The study also provides information on how surface modifiers of different molecular size interact with Pd nano-deposits. There are very few studies^{9, 28} on colloidal stabilization of NZVI with relatively low molecular weight surface modifiers such as RL, and no studies on effects of reactivity of Pd-NZVI by RL.

The effects of surface modifier type and dose on Pd-NZVI reactivity to TCE were evaluated by conducting a series of batch experiments where TCE degradation and end product formation were monitored over time. TCE was chosen as a target contaminant because it is widely used in industry and it is considered to be neurotoxic and carcinogenic^{29, 30}, and has been used as a model contaminant in several studies on NZVI or Pd-NZVI reactivity.^{20, 31, 32} Most studies in the literature have employed the pre-grafting approach in Pd-NZVI reactivity studies.^{14, 19, 33} Because in field applications, the post-grafting method of stabilizing nanoparticles is more easily scalable than the pre-grafting method¹, Pd-NZVI particles were post-grafted with surface modifiers in the reactivity experiments. Surface modifier concentrations were monitored by total organic carbon (TOC) measurements and relationships between sorbed surface modifier concentrations and the extent of palladium deposition on NZVI under different CMC and RL doses were characterized. The surface modifier concentrations were varied up to 167 mg TOC/g NZVI and included concentrations shown to be adequate for significantly enhancing Pd-NZVI transport.^{9, 34-36}

MATERIALS AND METHODS

Surface modifiers. Sodium salt of CMC (M.W. 700000 g mol⁻¹) was obtained from Sigma-Aldrich, while rhamnolipid JBR215 (mixture of di-rhamnolipid with M.W. 650 g mol⁻¹ and mono-rhamnolipid with M.W.

504 g mol⁻¹) was purchased from Jeneil Biosurfactant Co. (Saukville, WI). Stock solutions of CMC (5 g TOC/L) and RL (10 g TOC /L) were prepared in (DI) water.

Preparation of Pd-NZVI suspensions. Bare NZVI was obtained as stock slurry from Golder Associates Inc. (Montreal, Canada) who synthesized NZVI by ball-milling of granular iron. The slurry was vacuum-dried and stored under anaerobic conditions. The total iron content was 70% (w/w) as determined by ICP-OES analyses, while the Fe⁰ content was 45% (w/w) as determined by measurement of the mass of H₂ released upon acidification of the NZVI according to methods described elsewhere.³²

Surface modifier-coated Pd-NZVI suspensions were prepared in 63 mL vials which were used as batch reactors for the TCE degradation experiments. Bare NZVI particles were suspended in 40 mL N₂-purged DI water and sonicated for 10 min (Misonix sonicator, S-4000) to disperse the aggregated nanoparticles. The sonicated NZVI suspension was then mixed with CMC (13 to 167 mg TOC/g NZVI) or RL (13 to 133 mg TOC/g NZVI) and equilibrated for 20 h by mixing in an end-over-end rotator. The TOC of the supernatant after separation of NZVI particles was analyzed periodically for up to 72 h and no changes were detected after 20 h. The NZVI was separated by centrifugation (6500g, 20 min) and then retained in a vial by the use of a super magnet (K&J Magnetics Inc.) while the supernatant containing the unadsorbed surface modifier was decanted. The supernatant was then analyzed with a TOC analyzer.

After equilibration, an ethanolic solution of palladium acetate was added to bare or surface modifier-coated NZVI (Pd(O₂CCH₃)₂=1 wt.% of NZVI) and sonicated for 15 minutes in a bath sonicator to achieve deposition of Pd⁰ onto the NZVI particles. The final Pd-NZVI concentration was 150 mg/L. The Pd-NZVI was prepared in an anaerobic glove box (Coy Laboratories, Inc) filled with N₂ (99.9% purity). The freshly synthesized Pd-NZVI was immediately used for TCE degradation studies without removing the excess surface modifier in the solution.

Reactivity studies. TCE degradation experiments were commenced by adding TCE (>99.5% purity, Sigma-Aldrich) as a methanolic solution to the reaction vials containing 40 mL of surface modifier-coated Pd-NZVI suspension, and 23 mL headspace, to yield a total TCE concentration of 23 mg/L. The vials were sealed with Mininert valve-fitted, Teflon-lined caps.

The TCE addition was carried out in the anaerobic glove box. The reactors were then capped and continuously mixed using a table top shaker at 650 rpm at 22 ±1 °C. The reactors were sampled periodically and analyzed for TCE, ethane and ethene. Other reaction products such as acetylene, butenes and dichloroethylenes were not observed in GC-MS analyses (Clarus SQ-8, Perkin Elmer) of headspace samples.

Analytical methods. The TOC content of surface modifiers was determined using a TOC analyzer (Shimadzu Corp.) and 0.1 g/L TOC corresponds to 0.3 g/L mass concentration of CMC and 0.17 g/L of RL. To account for differences in molecular weights of both the surface modifiers investigated, TOC was used as the basis for comparison of surface modifier doses. TCE was quantified by direct injection of 300 μ L of reactor headspace into a Varian CP 3800 GC with flame ionization detector. Further details on GC operation are provided in the Supporting Information (SI).

Nanoparticle characterization. X-ray Photoelectron Spectroscopy (XPS) was performed for bare NZVI and surface modifier coated NZVI using a VG Escalab 3MKII instrument to characterize the surface oxide layer. Cryogenic-Transmission Electron Microscopy (Cryo-TEM) was performed on uncoated Pd-NZVI and RL and CMC-coated Pd-NZVI to observe the aggregate structure of nanoparticles in suspension. 3 μ L of sample (Pd-NZVI suspension, 1 g/L) was added to C-Flat 2/2 EM grids (Protochips). Further details on sample preparation and handling are provided in the SI.

High Resolution-Transmission Electron Microscopy (HR-TEM) was performed on uncoated Pd-NZVI particles to characterize the size of Pd⁰ on the NZVI, using a Tecnai G2F20 S/TEM, equipped with 4k \times 4k CCD Camera and operated at 200 kV.

The hydrodynamic diameters of coated and uncoated Pd-NZVI particles were determined by dynamic light scattering (Zetasizer Nano ZS, Malvern). Size measurements were done at regular intervals of time to assess the extent of aggregation of Pd-NZVI during TCE degradation. Identical mixing conditions and particle concentration (150 mg/L) were used and particle diameters were monitored over time periods equal to the duration as the reactivity studies.

The mass of Pd deposited on NZVI particles and free Pd in supernatant was measured using an ICP-OES (Thermo ICap Duo 6500). The surface modifier-coated Pd-NZVI was separated from solution using centrifugation followed by magnetic separation and then the nanoparticles and the supernatant were separately acid digested in aqua regia (3:1 HCl: HNO₃).

The mass of surface modifier adsorbed to the NZVI surface (i.e., particles to which Pd had not yet been added) was estimated by measuring the difference between the total surface modifier dose and the surface modifier remaining in the supernatant after equilibration (i.e., 20 h mixing period between NZVI and surface modifier). As mentioned earlier, the NZVI particles were separated from solution using centrifugation and magnetic separation.

Fourier transform infrared (FTIR) measurements were carried out on lyophilized RL- and CMC-coated NZVI particles, using a Thermo Nicolet 6500 mid-range instrument equipped with a DTGS detector. Samples were loaded onto a diffuse reflectance cell with a reflective gold booster. All spectra were collected with a resolution of 4 cm⁻¹ in the range of 4000-400 cm⁻¹.

RESULTS AND DISCUSSION

Characterization of Pd-NZVI. High resolution TEM images of Pd-NZVI particles confirmed the deposition of Pd on NZVI particles (confirmed through EDS shown in Figure S1). Primary sizes of NZVI particles ranged from 25-30 nm while Pd sites were deposited in a random fashion as islets of 3 nm in diameter (Figure 1. a1-a2). This is in good agreement with other studies which show Pd deposited as 2-4 nm discrete clusters.^{18, 37, 38}

XPS analyses revealed the presence of iron oxide and hydroxide species on the surface of bare NZVI and RL- and CMC- coated NZVI. Further details are provided in the SI.

Effect of surface modifier loading on TCE degradation rate. The amount of CMC or RL used to coat the Pd-NZVI particles was varied up to 167 mg TOC/g NZVI, in order to study the effect of surface modifier loadings on TCE degradation rates. The reaction vials had stoichiometrically excess Pd-NZVI relative to TCE.

Each data point in Figure 2 represents the pseudo first-order TCE degradation rate constant (k_{obs}) obtained from TCE degradation profiles (Figures S3 and S4) from triplicate reactors for each total surface modifier loading used. For RL loadings from 33 to 133 mg TOC/g NZVI, only the first three data points from time 0 were used to calculate the k_{obs} (Figure S3), as no further degradation was observed thereafter. The reason for this inhibition of reactivity is discussed in the following section. For all other cases of coated and uncoated Pd-NZVI, all the experimental data points were fitted to the pseudo first-order rate law ($r^2 > 0.98$) to determine k_{obs} . The k_{obs} values were corrected for partitioning of contaminant between aqueous and gaseous phases, using methods described elsewhere³⁹ and in the SI.

As observed in Figure 2, depending on their loading, the Pd-NZVI coated with the two surface modifiers show distinctively different effects on TCE degradation rates. Uncoated bare Pd-NZVI particles yielded a k_{obs} of 0.191(±0.001) h⁻¹, and coating the nanoparticles with varying concentrations of CMC did not have any significant effect on the TCE degradation rate constant (one-way ANOVA, $p > 0.05$). In contrast, increasing the RL loading in the reaction vials containing Pd-NZVI caused a progressively significant decrease in the k_{obs} . At

133 mg TOC RL/g NZVI, the TCE degradation rate was only $0.027(\pm 0.001) \text{ h}^{-1}$. Losses due to leakage from vial or sample handling were negligible and >90% mass balance of carbon was obtained for all systems (Figure S5). All experiments were carried out below the critical micellar concentration of RL (30 mg TOC/L⁹) and no partitioning of TCE to only RL or only CMC solutions were measured.

An important observation was made by Phenrat et al.²² in the context of non-palladized NZVI post-grafted with polyelectrolytes. The authors observed that the rate of TCE degradation decreased when polyelectrolytes were adsorbed to the NZVI surface and attributed it to the blocking of surface reactive sites at low concentrations of adsorbed polyelectrolytes (between 0.3 to 1.6 mg/m² surface excess, for different polyelectrolytes), and a combination of site blocking and reduced availability of aqueous TCE at the NZVI surface at higher surface excess concentrations. The role of site blocking with respect to Pd-NZVI in our study is discussed in a later section. However, the reduced availability of aqueous TCE at the Pd sites is unlikely because Pd nano-islets could only be deposited at sites which are not blocked by the adsorbed surface modifier coatings.

To investigate the differences in reactivity rates observed between bare Pd-NZVI and surface modified Pd-NZVI, three possible ways in which surface modifiers could potentially alter the reactivity of Pd-NZVI were investigated: (a) changes caused in aggregate sizes, (b) changes in Pd deposition on the NZVI particles in the presence of surface modifiers, and (c) interaction of surface modifier molecules in solution with the Pd-NZVI.

In previous studies, aggregation of NZVI particles has often been associated with a loss in contaminant degradation rates by NZVI, in that a loss of nanoparticle surface area due to aggregation results in a decrease in sites available for contaminant degradation.^{7, 40, 41} By stabilizing Pd-NZVI with surface modifiers, one would expect improved reactivity of Pd-NZVI due to the significantly smaller aggregate sizes and higher surface area than uncoated Pd-NZVI. The nanoparticle sizes were determined for uncoated Pd-NZVI, and coated Pd-NZVI at two different representative loadings for each type of surface modifier, at 13 mg TOC/g NZVI and 67 mg TOC/g NZVI, in order to probe whether surface modifier loading influenced the extent of Pd-NZVI stabilization which then caused the differences in the TCE degradation rate constants observed in Figure 2. Average diameters of uncoated Pd-NZVI particles were approximately 1500 nm whereas Pd-NZVI coated with both RL and CMC at the selected total surface modifier loadings were 300 nm (Table S2). Despite such significant differences in sizes between uncoated and coated Pd-NZVI, CMC-coatings did not improve Pd-NZVI reactivity while RL-coatings had an adverse effect on reactivity.

Because aggregate sizes did not correlate with changing degradation rates, the effect of sorption of surface modifiers to the NZVI surface on Pd deposition was probed along with the interaction of excess surface

modifier molecules with the Pd-NZVI. The lack of correlation between particle size and Pd-NZVI reactivity is also explored in a later section.

Palladium deposition studies. To investigate whether the presence of surface modifier adsorbed on the surface of NZVI can cause changes in Pd deposition, Pd mass loadings (% w/w NZVI) on NZVI surface were characterized at three different total surface modifier loadings: 13, 33 and 67 mg TOC/g NZVI. Figure 3 demonstrates the difference in the deposition of Pd on the NZVI particles by the two surface modifiers. The nominal dose of Pd on NZVI particles was 0.5% w/w of NZVI across all reactors with the different CMC and RL doses. However, as shown in Figure 3, Pd deposits on the NZVI to different extents when CMC and RL are used as surface modifiers. CMC has little effect on the deposition of 0.5% Pd (w/w NZVI) on the NZVI surface. In contrast, Pd deposited onto NZVI decreased with an increase in RL loading. The concentration of deposited Pd was $0.35(\pm 0.01)\%$ at 13 mg TOC/g NZVI which decreased to $0.13(\pm 0.02)\%$ at 67 mg TOC/g NZVI. For RL coated Pd-NZVI, a decrease in Pd deposition between 13 and 67 mg TOC/g NZVI corresponded to a decrease in TCE degradation rate constants from 0.145 h^{-1} to 0.045 h^{-1} , whereas for Pd-NZVI coated with CMC up to 167 mg TOC/g NZVI, no effect on TCE degradation or Pd deposition was observed, suggesting that changes in Pd deposition affects the reactivity of the coated Pd-NZVI particles. However it should be noted that at total RL loadings of 33 and 67 mg TOC/g NZVI, reactivity of Pd-NZVI is also affected by the presence of RL in solution in addition to changes in Pd loading, as discussed in the next section.

The differences in Pd deposition on RL-coated NZVI and CMC-coated NZVI may be attributable to differences in sorption of the two surface modifiers and the configuration of the surface modifier molecules on the NZVI surface, both of which could affect the number of reactive sites and surface area available for Pd deposition. Thus, the adsorption of the two surface modifiers on NZVI during the post-grafting process was verified using adsorption isotherm experiments. Figure 4a presents the amount of surface modifier adsorbed onto the NZVI particles at equilibrium as a function of total surface modifier loading. There is a significant difference in the affinity of the two coatings to the NZVI surface with the adsorption of RL being considerably higher than CMC. For instance, approximately 12 mg TOC of CMC/g NZVI was adsorbed at a total CMC loading of 67 mg TOC/g NZVI, whereas, 48 mg TOC of RL/g NZVI was adsorbed to NZVI at an identical total RL loading. Furthermore, it should be noted that CMC in solution exists at all surface modifier loadings investigated, while RL in solution was measured only at and above 33 mg TOC/g NZVI. To characterize the nature of bonding of CMC and RL onto NZVI surface, FTIR measurements were carried out on surface-modified NZVI particles coated with CMC or RL. Both CMC and RL were found to interact with the NZVI through the carboxylate group (Figures S6 and S7).

All RL was completely sorbed to NZVI surface for total RL doses up to 20 mg TOC/g NZVI, while the adsorption of RL to NZVI surface from loadings between 33-133 mg TOC/g NZVI could be described using the Langmuir isotherm as shown in Figure 4b. The adsorption of CMC to NZVI surface, at the surface modifier loadings employed, was best described using the Freundlich isotherm as shown in Figure 4c. It should be noted here that Phenrat et al.¹¹ found that 700K CMC sorption to NZVI was best described by a Langmuir isotherm. The difference in the adsorption behaviour of CMC to NZVI compared to our study may be due to differences in the solution chemistry (pH of 7.2 in our study versus pH range of 9.5 to 10.5 in theirs) and NZVI surface chemistry related to differences in particle synthesis methods. Nevertheless, NZVI particles in our study as well as by Phenrat et al. were negatively charged at the pH employed. CMC sorbs significantly less compared to RL and has a different sorption behavior as shown in Figure 4a and discussed above, likely due to differences in molecular size and structure (Table S1). Although CMC sorbed on NZVI, we observed no decrease in k_{obs} for CMC coated Pd-NZVI. This is likely due to limited blocking of Pd deposition sites on the NZVI due to a more open configuration (increased amounts of loops and tails) of the polyelectrolyte due to its macromolecular structure at higher concentrations.^{8, 22} In contrast, the significantly smaller RL molecules likely adsorb in a flat conformation and form a more compact coating on the NZVI surface.^{24, 42}

RL has been previously reported to complex with a number of different metal ions⁴³. Thus, we investigated the extent to which free RL in solution (present at total RL loadings of 33 to 133 mg TOC RL/g NZVI) complexed Pd^{2+} . In a separate experiment, we contacted uncoated NZVI and a suspension of RL- Pd^{2+} for 15 minutes (a time period which was insufficient for RL sorption to NZVI as determined by TOC analyses, but sufficient for Pd reduction and deposition on NZVI). The NZVI was then separated and analyzed by ICP-OES to quantify the amounts of Pd associated with the particles. Because no RL sorbed, the Pd associated with NZVI can be attributed to Pd^0 derived from the non-complexed Pd^{2+} in the RL- Pd^{2+} suspension. The amount of Pd^0 that did not deposit on NZVI was assumed to be complexed with RL. The experimental procedures are further explained in the SI and in Figure S8. Using the knowledge of the amounts of Pd complexed by RL in solution, we calculated that in a representative system having a total RL loading of 67 mg TOC RL/g NZVI, for a nominal dose of 0.03 mg Pd (0.5% w/w NZVI), (i) 0.009 mg Pd (0.15% w/w NZVI) was complexed by the 3 mg TOC/L RL in solution, while (ii) 0.0078 mg Pd (0.13% w/w NZVI) was deposited as Pd^0 on the NZVI surface coated with 48 mg TOC/g NZVI of RL, and (iii) 0.0132 mg Pd (0.22% w/w NZVI) remained in solution (not deposited) and as non-complexed Pd^{2+} . This suggests that surface sorbed RL plays a more significant role in controlling the overall Pd^0 deposition because a large fraction of non-complexed Pd^{2+} was unable to deposit on NZVI. The calculation are further explained in the SI.

Figure 5 presents a schematic showing these processes including the role of excess surface modifier in solution on TCE degradation, which is discussed below.

Effect of excess surface modifiers in solution on TCE degradation rate. For all CMC loadings and RL loadings of 13 and 20 mg TOC/g NZVI, all of the TCE in the vials was degraded in less than 40 h. However, at RL loadings of 33 to 133 mg TOC RL/g NZVI, less than 20% of the TCE was degraded over 7 h and thereafter there was no further degradation (Figure S3).

We investigated whether the incomplete degradation was associated with the presence of excess RL in solution at total loadings ranging from 33 to 133 mg TOC RL/g NZVI (Figure 4). We hypothesized that some of the RL in solution was able to coat the Pd⁰-nanodeposits after their formation and make the Pd⁰ unavailable for TCE dechlorination. This hypothesis was verified by (a) studying the sorption kinetics of RL to Pd⁰ surfaces (created by synthesizing Pd⁰ nanoparticles) and (b) conducting TCE degradation experiments with and without excess RL present in solution. The sorption of RL to Pd⁰ fitted a Langmuir isotherm (Figure S9), thus suggesting that coating of Pd⁰ deposits by RL from the solution phase can occur after formation of the Pd⁰ nanodeposits. To investigate the consequences of RL sorption to Pd⁰ on the reactivity of Pd-NZVI, two identical sets of reactors were prepared in which NZVI particles were first coated with 67 mg TOC of RL/g NZVI. After the NZVI particles had equilibrated with RL, Pd nano-deposits were formed by adding Pd-acetate. Then, one set of triplicate reactors was maintained as is (i.e. with excess RL in solution), while in the other set of triplicate reactors, the excess RL in solution was removed immediately after Pd⁰ deposition by decanting the supernatant (after centrifugation and retention of the Pd-NZVI particles using a supermagnet). The particles in the reactor set without RL in solution, were resuspended in fresh deionized water and subsequently tested for TCE degradation. It was confirmed with TOC analysis that RL did not desorb from the nanoparticles after the resuspension step. A schematic of the reactor sets tested for TCE degradation is shown in Figure 6b and 6c.

As shown in Figure 6a, the system without any RL in solution, was able to degrade TCE in the reactor completely, while the system with excess RL in solution was able to achieve only 20% reduction.

Therefore, changes in TCE degradation rates observed for Pd-NZVI coated with RL is caused by two processes: (a) reduction in Pd deposition caused due to sorption of RL to NZVI surface, and (b) coating of deposited Pd⁰ by the excess RL from the solution phase. The amounts of deposited Pd have been discussed earlier and are shown in Figure 3. Depending on the total loading of RL, either one or both processes may be

involved in altering the reactivity of Pd-NZVI. Conversely, CMC adsorbed to NZVI surface or present in solution do not affect the reaction rates of Pd-NZVI particles. A schematic outlining the effects of the two surface modifiers on Pd-NZVI is presented in Figure 5.

Aggregation and reactivity. The lack of relationship between aggregate sizes and Pd-NZVI reactivity was further probed by carrying out Cryo-TEM analysis on suspension droplets of uncoated and coated Pd-NZVI particles, in order to observe their aggregate morphology *in solution*. Cryo-TEM avoids the artefacts associated with drying of the sample which may result in aggregation of nanoparticles during sample preparation for regular TEM imaging. Images show that uncoated Pd-NZVI formed large (~900 nm), open, porous aggregate structures in solution whereas RL- or CMC-coated Pd-NZVI formed smaller (~200 nm) aggregates of fewer nanoparticles (Figure 1. b1-b3). Given the open and porous morphology of the Pd-NZVI aggregates, the degradation rate of TCE by Pd-NZVI is more likely to be dependent on the mass loading of Pd on NZVI rather than aggregate size, because access of TCE to the Pd sites (where TCE degradation primarily takes place¹⁸) is unlikely to be hindered with increase in aggregate size.

He and Zhao¹⁹ reported that changes in CMC-coated Pd-NZVI particle sizes from 200 to 18.6 nm (11 times increase in surface area) did not proportionately enhance reactivity rates (1.7 times increase). Additionally, our analysis of their graphical data reveals that there was no statistical difference (one-way ANOVA, $p > 0.05$) in the TCE degradation rate constants for CMC-coated Pd-NZVI with CMC:Fe molar ratios of 0.0093 to 0.0186. The authors observed a statistically significant decrease in rate constants only at a high CMC:Fe ratio of 0.061, a dose much higher than those used in our study. Sakulchaicharoen et al.¹⁴ also reported only a 1.3 fold increase in TCE degradation rate constant for CMC-coated Pd-NZVI sizes between 18.8 nm and 2.4 nm (7.7 times increase in specific surface area). It should be noted that He and Zhao¹⁹ observed a 8 fold lower reactivity rate of uncoated Pd-NZVI compared to CMC-coated Pd-NZVI. That difference in reactivity is likely due to the different morphology and composition of the uncoated NZVI, which had a dendritic, floc-like morphology, compared to the CMC-coated particles which existed as solid, spherical particles.^{7, 8} However, because the authors did not measure the Pd mass deposition, it is difficult to ascertain the exact reasons for differences in reactivity. In this study, the uncoated and coated non-palladized NZVI had an identical composition as CMC was post-grafted, and thus the only changes that occurred upon CMC-coating was the change in aggregation state as shown in Figure 1 (b1-b3), which did not alter the reactivity of the particles to TCE.

IMPLICATIONS

A number of different studies in the literature have focused on reducing Pd-NZVI aggregate size to enhance mobility in the subsurface as well as improve their reactivity to target contaminants. We have demonstrated through this study, that aggregate morphology rather than size plays an important role in determining Pd-NZVI reactivity. A significant factor determining Pd-NZVI reactivity is its interaction with the stabilizing surface modifiers. In this study, the relationship between surface modifiers types and doses and reactivity was studied in batch reactors, and further studies of these interactions in packed sand columns and tanks under NZVI injection conditions are needed to determine optimal surface modifier doses.

Rhamnolipids are very efficient for enhancing Pd-NZVI transport in the subsurface⁹, thus it was of interest to us to measure the transport effectiveness of RL at the low loading of 13 mg TOC/g NZVI (Figure S10), where its reactivity is not suppressed. Even at such low concentrations, RL is able to significantly enhance transport compared to CMC-coated Pd-NZVI with an identical surface modifier loading or bare Pd-NZVI. Thus, for overall efficient remediation, low concentrations of RL are desirable as they provide high reactivity and efficient transport of Pd-NZVI. For CMC coated Pd-NZVI, the CMC dose may be chosen solely based on effects on transport potential.

SUPPORTING INFORMATION

Details on GC, XPS, Cryo-TEM methods; XPS and FTIR data discussion; TCE degradation time profiles and reaction end product distribution graphs, and RL- and CM- coated Pd-NZVI transport experiments.

ACKNOWLEDGEMENTS

This research was supported by the NSERC, Canada (Grant Nos. STPGP 365253-08; 203158-11 and 413978-12), Golder Associates Inc., and the FRQ-NT, Quebec, Canada (Grant No. 147187). We thank Ranjan Roy and Andrew Golsztajn (McGill) for assisting with FTIR, TOC and ICP measurements; Kaustuv Basu, Hojatollah Vali, S. Kelly Sears (McGill) for the Cryo-TEM analysis; and J. Lefebvre (Polytechnique Montréal) for XPS analyses. S.B. and M.B. were supported by McGill Engineering Doctoral Awards.

REFERENCES

1. O'Carroll, D.; Sleep, B.; Krol, M.; Boparai, H.; Kocur, C., Nanoscale zero valent iron and bimetallic particles for contaminated site remediation. *Adv. Water Resour.* **2013**, *51*, 104-122.
2. Reardon, E. J.; Fagan, R.; Vogan, J. L.; Przepiora, A., Anaerobic corrosion reaction kinetics of nanosized iron. *Environ. Sci. Technol.* **2008**, *42*, (7), 2420-2425.
3. Sarathy, V.; Tratnyek, P. G.; Nurmi, J. T.; Baer, D. R.; Amonette, J. E.; Chun, C. L.; Penn, R. L.; Reardon, E. J., Aging of iron nanoparticles in aqueous solution: effects on structure and reactivity. *J. Phys. Chem. C* **2008**, *112*, (7), 2286-2293.
4. Phenrat, T.; Saleh, N.; Sirk, K.; Tilton, R. D.; Lowry, G. V., Aggregation and sedimentation of aqueous nanoscale zerovalent iron dispersions. *Environ. Sci. Technol.* **2007**, *41*, (1), 284-290.
5. Dalla Vecchia, E.; Coisson, M.; Appino, C.; Vinai, F.; Sethi, R., Magnetic characterization and interaction modeling of zerovalent iron nanoparticles for the remediation of contaminated aquifers. *J. Nanosci. Nanotechnol.* **2009**, *9*, (5), 3210-3218.
6. Saleh, N.; Sirk, K.; Liu, Y.; Phenrat, T.; Dufour, B.; Matyjaszewski, K.; Tilton, R. D.; Lowry, G. V., Surface modifications enhance nanoiron transport and NAPL targeting in saturated porous media. *Environ. Eng. Sci.* **2007**, *24*, (1), 45-57.
7. He, F.; Zhao, D., Preparation and characterization of a new class of starch-stabilized bimetallic nanoparticles for degradation of chlorinated hydrocarbons in water. *Environ. Sci. Technol.* **2005**, *39*, (9), 3314-3320.
8. He, F.; Zhao, D.; Liu, J.; Roberts, C. B., Stabilization of Fe-Pd nanoparticles with sodium carboxymethyl cellulose for enhanced transport and dechlorination of trichloroethylene in soil and groundwater. *Ind. Eng. Chem. Res.* **2007**, *46*, (1), 29-34.
9. Basnet, M.; Ghoshal, S.; Tufenkji, N., Rhamnolipid biosurfactant and soy protein act as effective stabilizers in the aggregation and transport of palladium-doped zerovalent iron nanoparticles in saturated porous media. *Environ. Sci. Technol.* **2013**, *47*, (23), 13355-13364.
10. Cirtiu, C. M.; Raychoudhury, T.; Ghoshal, S.; Moores, A., Systematic comparison of the size, surface characteristics and colloidal stability of zero valent iron nanoparticles pre-and post-grafted with common polymers. *Colloids Surf. Physicochem. Eng. Aspects* **2011**, *390*, (1), 95-104.
11. Phenrat, T.; Saleh, N.; Sirk, K.; Kim, H.-J.; Tilton, R. D.; Lowry, G. V., Stabilization of aqueous nanoscale zerovalent iron dispersions by anionic polyelectrolytes: adsorbed anionic polyelectrolyte layer properties and their effect on aggregation and sedimentation. *J. Nanopart. Res.* **2008**, *10*, (5), 795-814.
12. Petosa, A. R.; Jaisi, D. P.; Quevedo, I. R.; Elimelech, M.; Tufenkji, N., Aggregation and deposition of engineered nanomaterials in aquatic environments: role of physicochemical interactions. *Environ. Sci. Technol.* **2010**, *44*, (17), 6532-6549.
13. Lien, H.-L.; Zhang, W.-x., Nanoscale iron particles for complete reduction of chlorinated ethenes. *Colloids Surf. Physicochem. Eng. Aspects* **2001**, *191*, (1), 97-105.
14. Sakulchaicharoen, N.; O'Carroll, D. M.; Herrera, J. E., Enhanced stability and dechlorination activity of pre-synthesis stabilized nanoscale FePd particles. *J. Contam. Hydrol.* **2010**, *118*, (3), 117-127.
15. Lien, H.-L.; Zhang, W.-X., Nanoscale Pd/Fe bimetallic particles: catalytic effects of palladium on hydrodechlorination. *Appl. Catal., B* **2007**, *77*, (1), 110-116.
16. Lien, H.; Zhang, W., Effect of palladium on the reductive dechlorination of chlorinated ethylenes with nanoscale Pd/Fe particles. *Water Supply* **2005**, *4*, (5-6), 297-303.
17. Zhu, B.-W.; Lim, T.-T., Catalytic reduction of chlorobenzenes with Pd/Fe nanoparticles: reactive sites, catalyst stability, particle aging, and regeneration. *Environ. Sci. Technol.* **2007**, *41*, (21), 7523-7529.

18. Xie, Y.; Cwiertny, D. M., Chlorinated solvent transformation by palladized zerovalent iron: Mechanistic insights from reductant loading studies and solvent kinetic isotope effects. *Environ. Sci. Technol.* **2013**, *47*, (14), 7940-7948.
19. He, F.; Zhao, D., Hydrodechlorination of trichloroethene using stabilized Fe-Pd nanoparticles: Reaction mechanism and effects of stabilizers, catalysts and reaction conditions. *Appl. Catal., B* **2008**, *84*, (3), 533-540.
20. Cho, Y.; Choi, S.-I., Degradation of PCE, TCE and 1, 1, 1-TCA by nanosized FePd bimetallic particles under various experimental conditions. *Chemosphere* **2010**, *81*, (7), 940-945.
21. Zhou, H.; Han, J.; Baig, S. A.; Xu, X., Dechlorination of 2,4-dichlorophenoxyacetic acid by sodium carboxymethyl cellulose-stabilized Pd/Fe nanoparticles. *J. Hazard. Mater.* **2011**, *198*, 7-12.
22. Phenrat, T.; Liu, Y.; Tilton, R. D.; Lowry, G. V., Adsorbed polyelectrolyte coatings decrease Fe0 nanoparticle reactivity with TCE in water: conceptual model and mechanisms. *Environ. Sci. Technol.* **2009**, *43*, (5), 1507-1514.
23. Sun, Y.-P.; Li, X.-Q.; Zhang, W.-X.; Wang, H. P., A method for the preparation of stable dispersion of zero-valent iron nanoparticles. *Colloids Surf. Physicochem. Eng. Aspects* **2007**, *308*, (1), 60-66.
24. Zhu, B.-W.; Lim, T.-T.; Feng, J., Influences of amphiphiles on dechlorination of a trichlorobenzene by nanoscale Pd/Fe: adsorption, reaction kinetics, and interfacial interactions. *Environ. Sci. Technol.* **2008**, *42*, (12), 4513-4519.
25. Basnet, M.; Di Tommaso, C.; Ghoshal, S.; Tufenkji, N., Reduced transport potential of a palladium-doped zero valent iron nanoparticle in a water saturated loamy sand. *Water research* **2015**, *68*, 354-363.
26. Fatisson, J.; Ghoshal, S.; Tufenkji, N., Deposition of carboxymethylcellulose-coated zero-valent iron nanoparticles onto silica: Roles of solution chemistry and organic molecules. *Langmuir* **2010**, *26*, (15), 12832-12840.
27. Raychoudhury, T.; Naja, G.; Ghoshal, S., Assessment of transport of two polyelectrolyte-stabilized zero-valent iron nanoparticles in porous media. *J. Contam. Hydrol.* **2010**, *118*, (3), 143-151.
28. Saleh, N.; Kim, H.-J.; Phenrat, T.; Matyjaszewski, K.; Tilton, R. D.; Lowry, G. V., Ionic strength and composition affect the mobility of surface-modified Fe0 nanoparticles in water-saturated sand columns. *Environ. Sci. Technol.* **2008**, *42*, (9), 3349-3355.
29. Goldman, S. M., Trichloroethylene and Parkinson's disease: dissolving the puzzle. **2010**.
30. Caldwell, J. C.; Keshava, N., Key issues in the modes of action and effects of trichloroethylene metabolites for liver and kidney tumorigenesis. *Environ. Health Perspect.* **2006**, 1457-1463.
31. Kim, Y. H.; Carraway, E., Reductive dechlorination of TCE by zero valent bimetals. *Environ. Technol.* **2003**, *24*, (1), 69-75.
32. Liu, Y.; Majetich, S. A.; Tilton, R. D.; Sholl, D. S.; Lowry, G. V., TCE dechlorination rates, pathways, and efficiency of nanoscale iron particles with different properties. *Environ. Sci. Technol.* **2005**, *39*, (5), 1338-1345.
33. He, F.; Zhao, D., Manipulating the size and dispersibility of zerovalent iron nanoparticles by use of carboxymethyl cellulose stabilizers. *Environ. Sci. Technol.* **2007**, *41*, (17), 6216-6221.
34. Kim, H.-J.; Phenrat, T.; Tilton, R. D.; Lowry, G. V., Fe0 nanoparticles remain mobile in porous media after aging due to slow desorption of polymeric surface modifiers. *Environ. Sci. Technol.* **2009**, *43*, (10), 3824-3830.
35. Phenrat, T.; Kim, H.-J.; Fagerlund, F.; Illangasekare, T.; Tilton, R. D.; Lowry, G. V., Particle size distribution, concentration, and magnetic attraction affect transport of polymer-modified Fe0 nanoparticles in sand columns. *Environ. Sci. Technol.* **2009**, *43*, (13), 5079-5085.
36. Jiemvarangkul, P.; Zhang, W.-x.; Lien, H.-L., Enhanced transport of polyelectrolyte stabilized nanoscale zero-valent iron (nZVI) in porous media. *Chem. Eng. J.* **2011**, *170*, (2), 482-491.

37. Yan, W.; Herzing, A. A.; Li, X.-q.; Kiely, C. J.; Zhang, W.-x., Structural evolution of Pd-doped nanoscale zero-valent iron (nZVI) in aqueous media and implications for particle aging and reactivity. *Environ. Sci. Technol.* **2010**, *44*, (11), 4288-4294.
38. Ling, L.; Zhang, W.-X., Structures of Pd–Fe (0) bimetallic nanoparticles near 0.1 nm resolution. *RSC Adv.* **2014**, *4*, (64), 33861-33865.
39. Burris, D. R.; Delcomyn, C. A.; Smith, M. H.; Roberts, A. L., Reductive dechlorination of tetrachloroethylene and trichloroethylene catalyzed by vitamin B12 in homogeneous and heterogeneous systems. *Environ. Sci. Technol.* **1996**, *30*, (10), 3047-3052.
40. Wang, C.-B.; Zhang, W.-X., Synthesizing nanoscale iron particles for rapid and complete dechlorination of TCE and PCBs. *Environ. Sci. Technol.* **1997**, *31*, (7), 2154-2156.
41. Lowry, G. V.; Gregory, K. B.; Apte, S. C.; Lead, J. R., Transformations of nanomaterials in the environment. *Environ. Sci. Technol.* **2012**, *46*, (13), 6893-6899.
42. Scamehorn, J.; Schechter, R.; Wade, W., Adsorption of surfactants on mineral oxide surfaces from aqueous solutions: I: Isomerically pure anionic surfactants. *J. Colloid Interface Sci.* **1982**, *85*, (2), 463-478.
43. Ochoa-Loza, F. J.; Artiola, J. F.; Maier, R. M., Stability constants for the complexation of various metals with a rhamnolipid biosurfactant. *J. Environ. Qual.* **2001**, *30*, (2), 479-485.

List of Figures:

Figure 1: (a1-a2) HR-TEM of uncoated Pd-NZVI (b1) Cryo TEM of uncoated Pd-NZVI (b2) Cryo TEM of RL-coated-Pd-NZVI (b3) Cryo TEM of CMC-coated-Pd-NZVI

Figure 2: Pseudo first order TCE degradation rate constants for Pd-NZVI at different surface modifier loadings in the reaction systems. Error bars represent standard deviation of measurements from triplicate reactors

Figure 3: Effect of surface modifier type and dose on palladium deposition. Error bars on histograms represent standard deviation of triplicates. Texts in bold alongside the histogram represent the TCE degradation rate constants obtained with Pd-NZVI particles at a given total surface modifier loading. The remainder of undeposited palladium was measured in the supernatant and >99% mass balance was obtained.

Figure 4: (a) Adsorbed surface modifier amounts with varying total surface modifier loadings. Solid lines are drawn to guide the eye. (b) RL adsorption to NZVI fitted with Langmuir isotherm, where q_e is the equilibrium adsorption capacity of NZVI, C_e is the equilibrium aqueous phase concentration of RL, q_m is the maximum adsorption capacity of NZVI and K_a is the adsorption equilibrium constant (c) CMC adsorption to NZVI fitted with Freundlich isotherm, where K_F and n are empirical constants. Error bars represent standard deviation of triplicates.

Figure 5: Schematic illustrating Pd-NZVI interactions in (a) absence of any surface modifier, (b) at low and high CMC loadings, (c) at low RL loading and, (d) at high RL loading

Figure 6: (a) TCE degradation by RL coated Pd-NZVI particles in the presence and absence of excess RL in solution. Error bars represent standard deviation of triplicates. Lines through data points are drawn to guide the eye. (b) Schematic of Pd, RL and Pd-NZVI interactions in the presence of RL in solution (c) Schematic of Pd, RL and Pd-NZVI interactions and TCE reactions in the absence of RL in solution.

Figure 1:

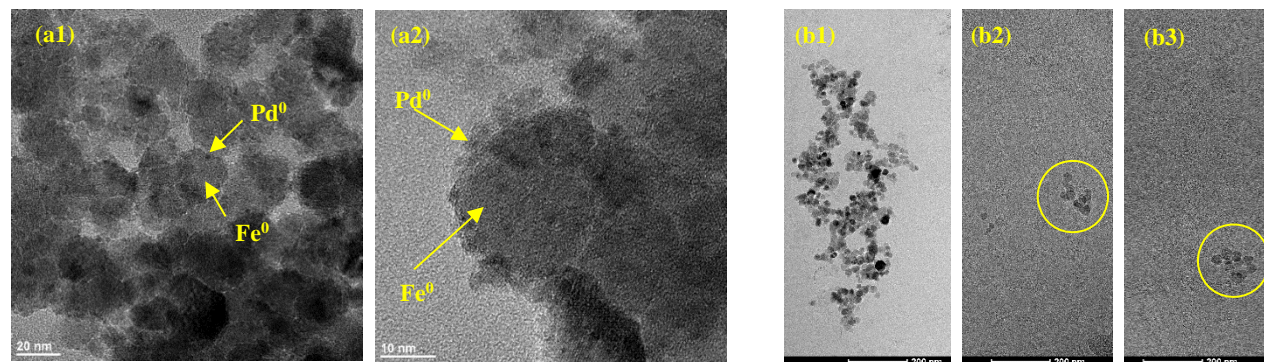


Figure 2:

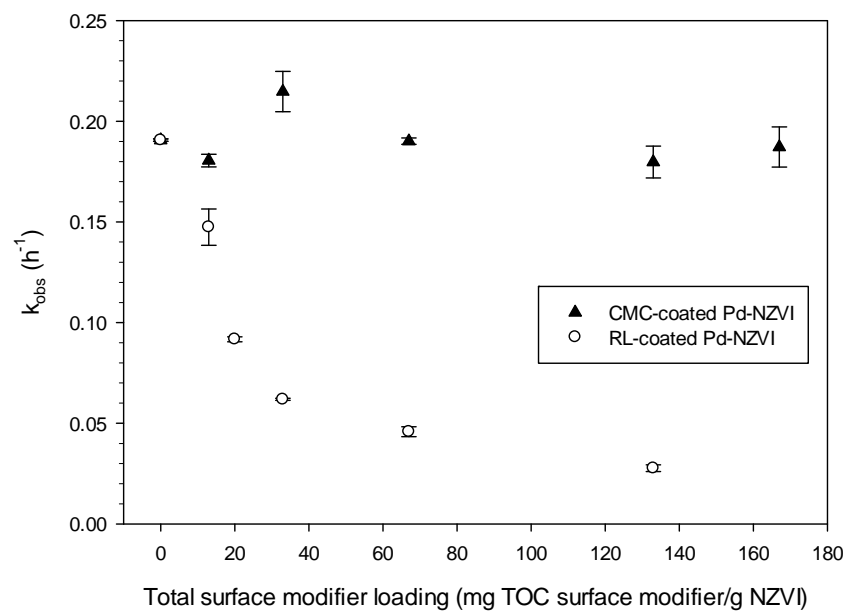


Figure 3:

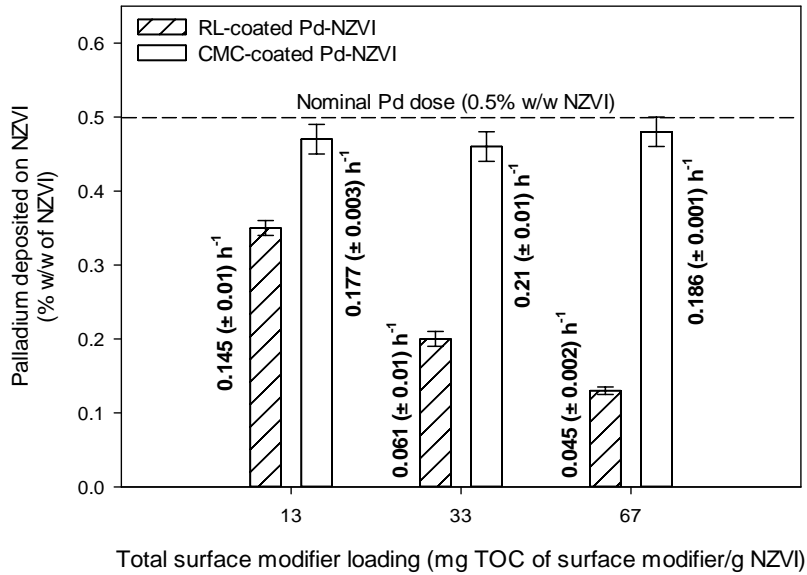


Figure 4:

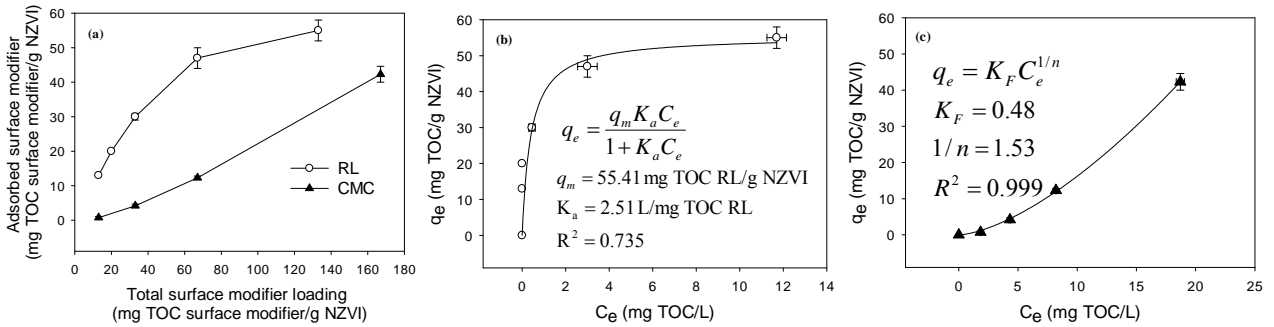
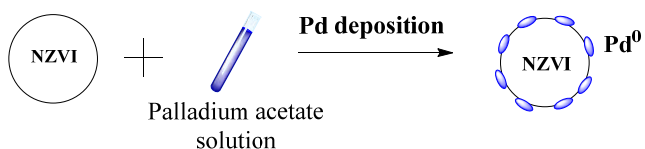
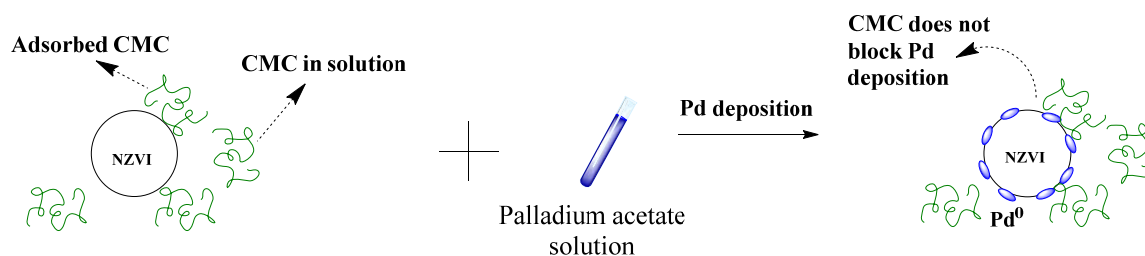


Figure 5:

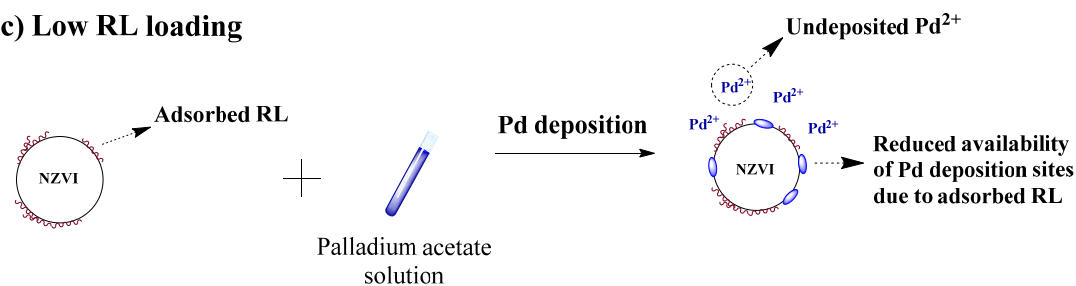
(a) Pd-NZVI



(b) Low and high CMC loading



(c) Low RL loading



(d) High RL loading

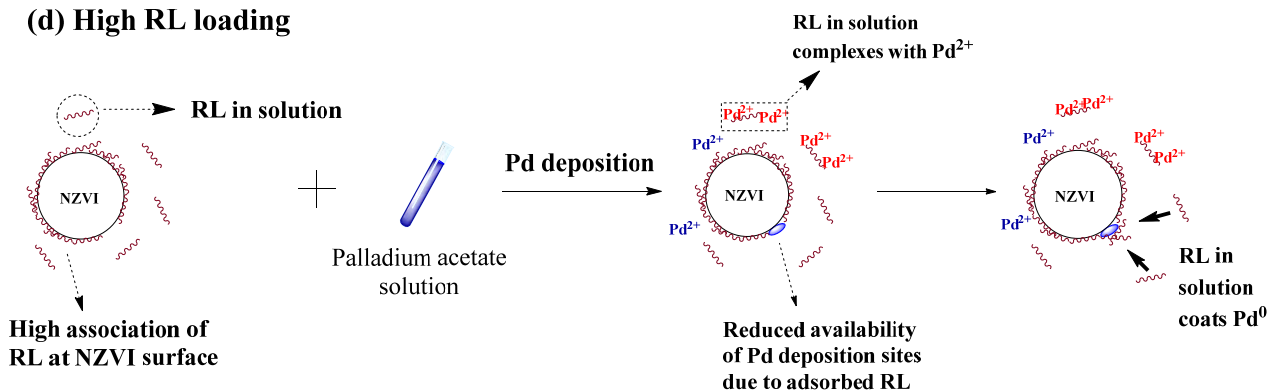
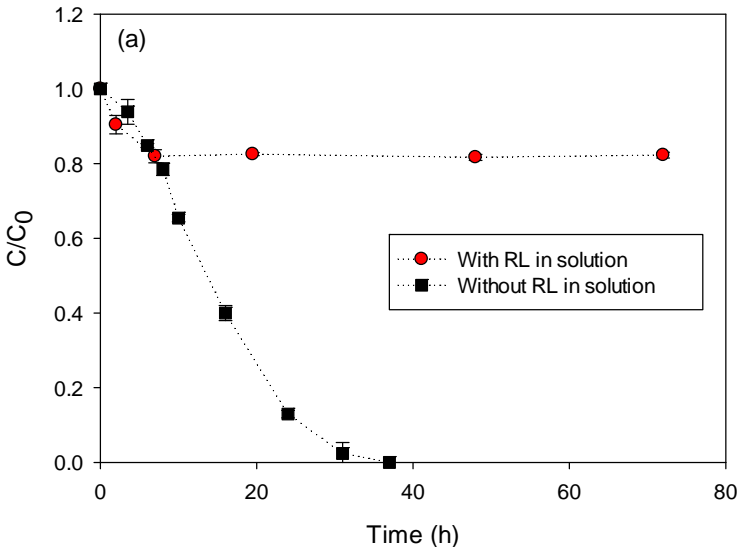
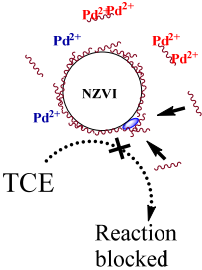


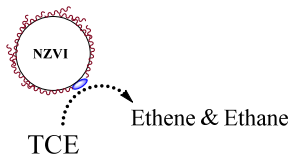
Figure 6:

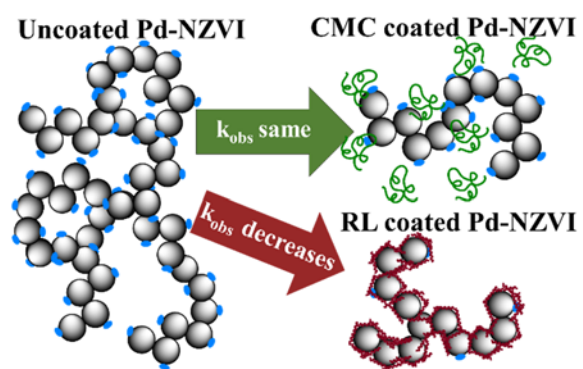


(b) With RL in solution



(c) Without RL in solution





Supporting Information

Effects of rhamnolipid and carboxymethylcellulose coatings on reactivity of palladium-doped nanoscale zerovalent iron particles

Sourjya Bhattacharjee¹, Mohan Basnet², Nathalie Tufenkji², Subhasis Ghoshal^{1*}

¹Department of Civil Engineering, McGill University, Montreal, QC H3A 0C3, Canada

²Department of Chemical Engineering, McGill University, Montreal, QC H3A 0C5, Canada

Number of pages: 11

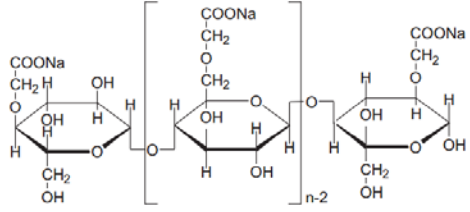
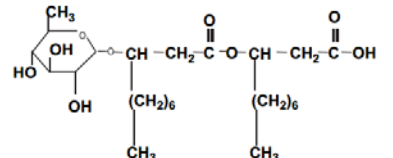
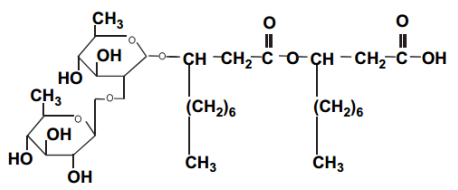
Number of tables: 2

Number of figures: 10

Journal: Environmental Science and Technology

*Corresponding author phone: 514-398-6867; fax: 514-398-7361; email: subhasis.ghoshal@mcgill.ca

Table S1: Details of surface modifiers used in the study. Structure of CMC adapted from Cirtiu et al.¹ and structure of RL adapted from Mulligan².

Surface Modifier	Composition	Molecular weight	Structure
Carboxymethyl-cellulose (CMC)	polyelectrolyte with sodium as a counter ion to the carboxyl group	700 kDa	
Rhamnolipid (RL)	aqueous solution containing mixture of mono- and dirhamnolipid	mono-RL: 504 Da di-RL: 650 Da	<p>mono-RL</p>  <p>di-RL</p> 

METHODS

GC-FID:

TCE was quantified by direct injection of 300 μ L of reactor headspace into a Varian CP 3800 GC with flame ionization detector fitted with a GS-Q plot column (0.53 mm \times 30 m, Agilent). 1000 ppm calibration gas standard of ethane, ethene and acetylene was obtained in nitrogen from Scotty Specialty Gases. Samples were injected in split-less mode at 250° C injector temperature and oven temperature held at 50°C for 2 min, followed by a ramp of 40 °C/min to 200 °C and then held at that temperature for 5 min.

X-ray Photoelectron Spectroscopy (XPS):

XPS was performed for bare NZVI using a VG Escalab 3MKII instrument to characterize the surface oxide layer. Dried NZVI was irradiated using an Al K α source at a power of 300 W (15 kV, 20 mA). The binding energies of the photoelectrons were calibrated by the aliphatic adventitious hydrocarbon C 1s peak at 285.0 eV with survey scan of energy step of 1.0 eV, pass energy of 100 eV and high resolution scans with energy step of 0.05 eV, pass energy of 20 eV.

Cryogenic-Transmission Electron Microscopy:

Cryogenic-Transmission electron microscopy (Cryo-TEM) was performed on uncoated Pd-NZVI and RL and CMC-coated Pd-NZVI to observe the aggregate structure of nanoparticles in solution. 3 μ L of sample

(Pd-NZVI suspension -1 g/L) was added to C-Flat 2/2 EM grids (Protochips). Excess fluid was blotted and the sample was flash frozen hydrated by plunging into a bath of liquid ethane using FEI Vitrobot Grid Plunging System (FEI electron optics). The grids were then stored in liquid nitrogen until observation. Images were acquired using FEI Titan Krios 300kv CryoS/TEM microscope (FEI,Inc) equipped with Falcon 2 Direct Detection Device (DDD)(FEI) at a magnification of 29000 \times corresponding to a 2.84 Å pixel size of (defocus level ranging from -2.0 to $-3.0\mu\text{m}$) under low dose conditions.

RESULTS AND DISCUSSION

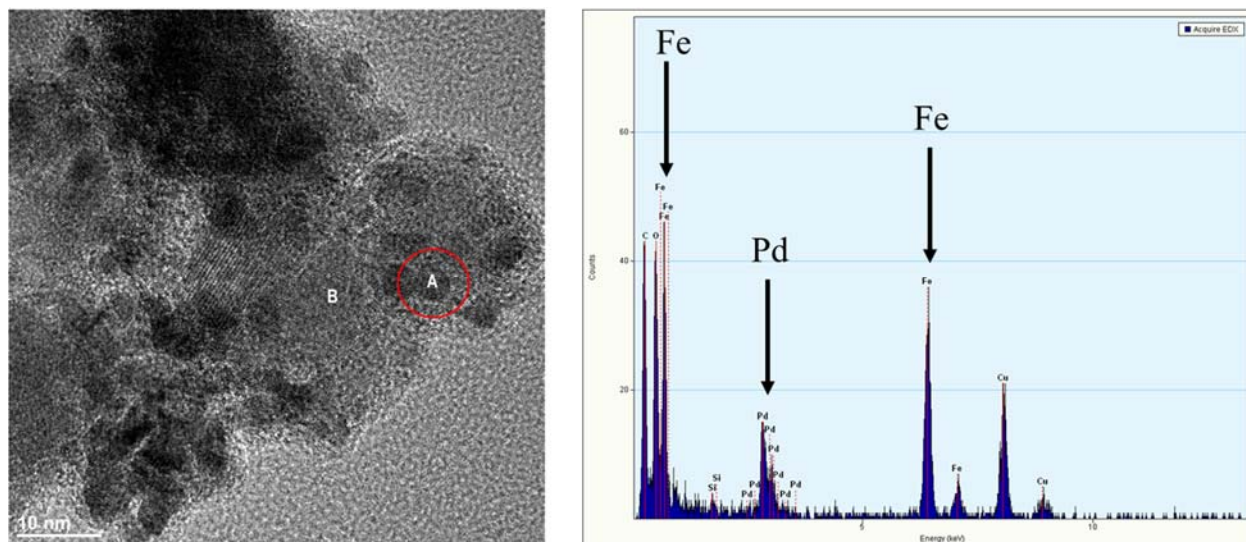


Figure S1: TEM-EDS performed on spot A of uncoated Pd-NZVI (spectra shown in right hand image)

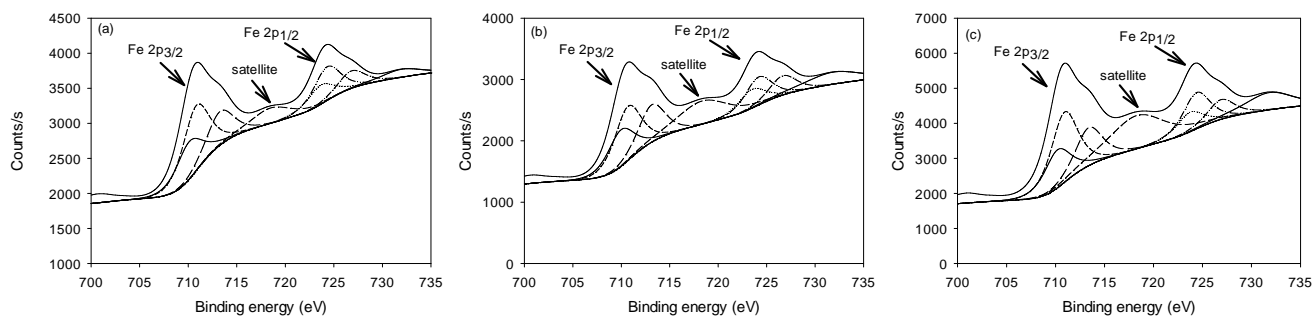


Figure S2: Narrow scans of Fe2p XPS spectra for (a) Uncoated NZVI (b) RL-coated NZVI (c) CMC-coated NZVI

X-ray Photoelectron Spectroscopy (XPS)

XPS analyses were conducted for uncoated NZVI, RL-coated NZVI and CMC-coated NZVI as shown in Figure S2 (a), (b) and (c) respectively. The spectra of RL-coated and CMC-coated NZVI were similar to the uncoated NZVI indicating that coating with surface modifiers did not alter the chemical state of the NZVI.

The low resolution spectra for uncoated NZVI indicated the presence of Fe and O on the surface. Based on high resolution scans for the Fe 2p_{3/2} spectra (Figure S1 a), deconvoluted peaks were obtained for Fe(II) and Fe(III) oxidation states between 710.0 eV and 713.3 eV. Peaks with binding energies of 710.1, 710.8 and 713.3 suggest the presence of FeO, Fe₂O₃ and FeOOH.^{3,4} No signal was detected for Fe(0) and can be attributed to the fact that X-ray probing depth was less than 5 nm. High resolution scans for oxygen (data not shown) reveal peaks at binding energies of 530.3 and 531.9 which also suggest the formation of oxide and hydroxide species of Fe.³

Electrophoretic mobility and Zeta potential:

Electrophoretic mobility (EPM) and zeta potential (ZP) of the NZVI particles used in this study have been previously reported⁵ and for 3 mM NaCl ionic strength and a pH of 7.7±0.2, an EPM of -1.9 ± 0.3 µm.cm/V.s was obtained for which the equivalent ZP was calculated as -26.4±3.4 mV.

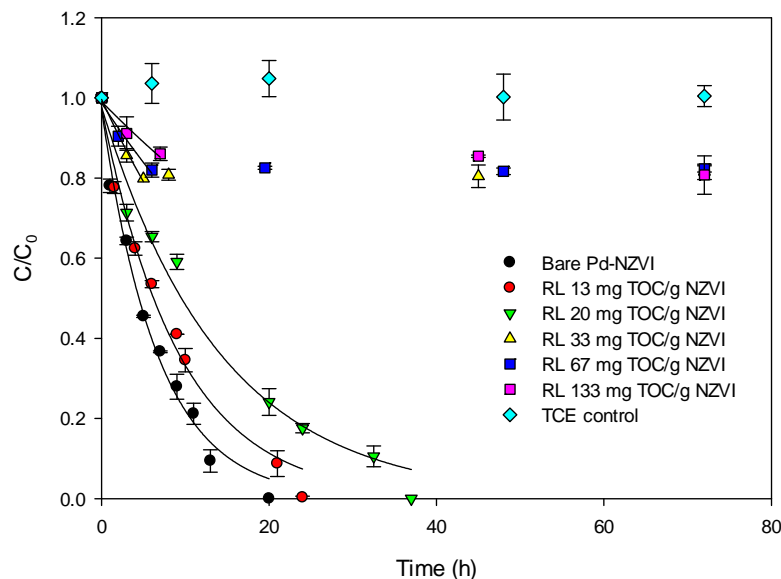


Figure S3: TCE degradation profiles as a function of time for RL-coated Pd-NZVI particles at different total RL loadings. Error bars represent standard deviation of triplicates. Lines through the data points are pseudo first order fits ($r^2 > 0.98$). For RL loadings 33 to 133 mg TOC/g NZVI, only first three data points were fitted to the model (where $r^2 > 0.98$) due to no further degradation beyond the initial time points.

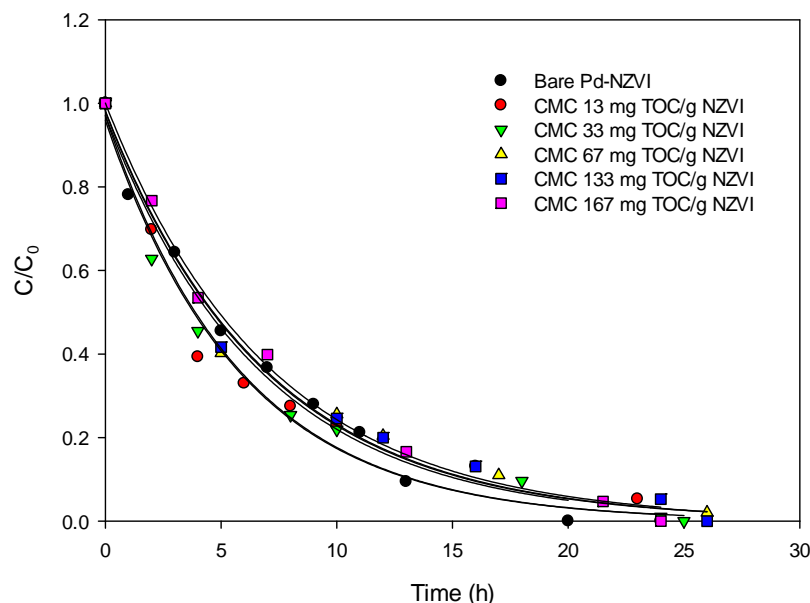


Figure S4: TCE degradation profiles as a function of time for CMC-coated Pd-NZVI particles at different polyelectrolyte loadings. Error bars represent standard deviation of triplicates. Lines through the data points are pseudo first order fits ($r^2 > 0.98$).

Calculation of k_{obs}

Values of k_{obs} were corrected as described in other studies^{6,7} to account for the effects of partitioning of the reactant between the aqueous and gas phases, using the following equation:

$$k_{obs} = k'_{obs} \left(1 + \frac{V_g}{V_w} K_H \right) \quad (S1)$$

where, k'_{obs} is the pseudo-first-order rate constants determined by best fit of measured aqueous concentrations as a function of time to a pseudo first-order rate law, while, V_w , V_g and K_H are the aqueous volume, headspace volume and the dimensionless Henry's coefficient.

Table S2: DLS hydrodynamic diameters for Pd-NZVI particles at different times in DI water

Time (h)	Hydrodynamic diameters (nm)				
	Uncoated Pd-NZVI	RL-Pd-NZVI		CMC-Pd-NZVI	
		13 mg TOC/g NZVI	67 mg TOC/g NZVI	13 mg TOC/g NZVI	67 mg TOC/g NZVI
5	1000±107	215±14	305±15	289±10	329±86
15	1566±303	323±76	300±56	375±80	340±72
40	1600±208	293±109	297±50	295±25	338±54

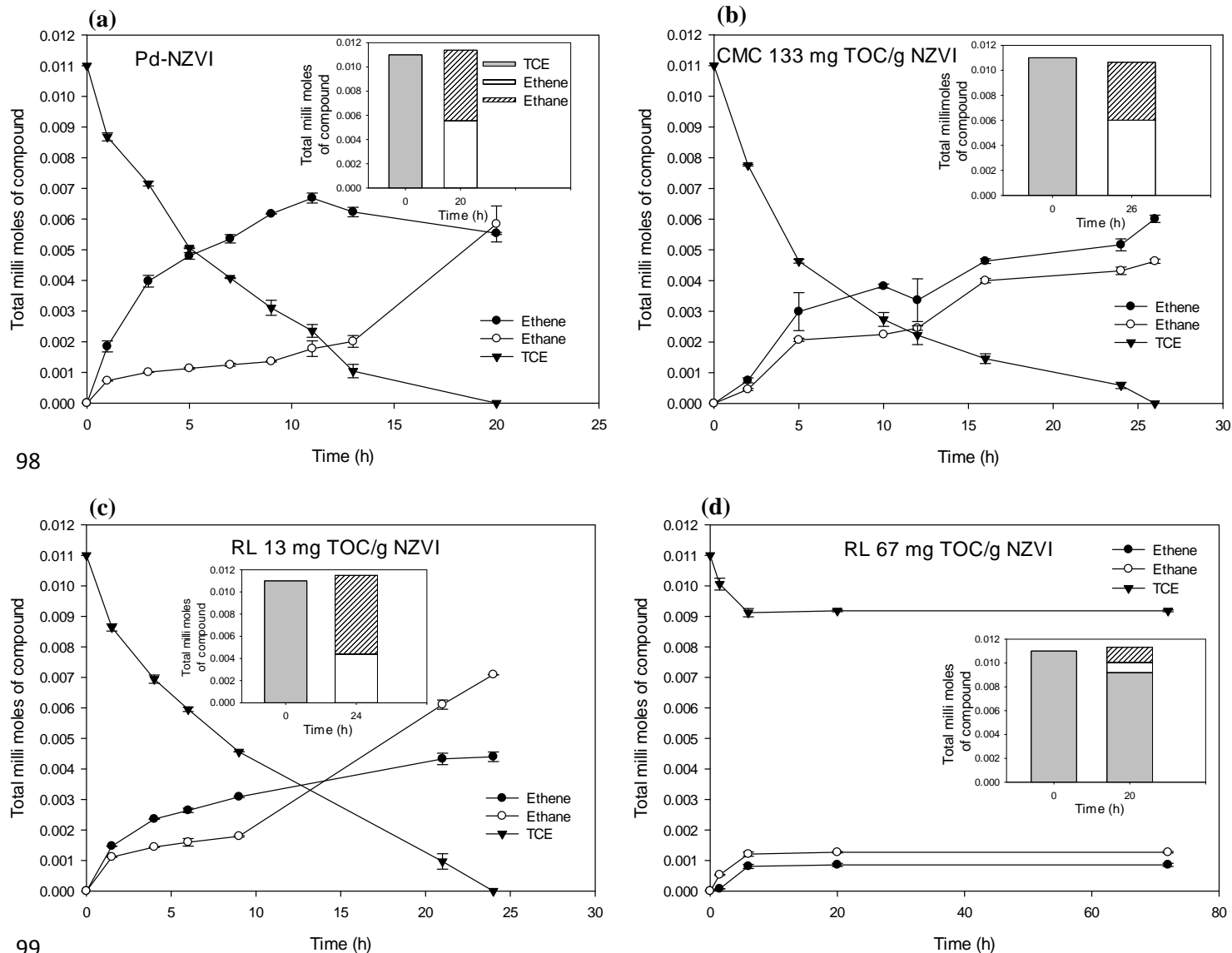


Figure S5: TCE degradation and end product evolution time profile for (a) Pd-NZVI (b) CMC-coated Pd-NZVI at total CMC loading of 133 mg TOC/g NZVI (c) Rhamnolipid-coated Pd-NZVI at total RL loading of 13 mg TOC/g NZVI (d) Rhamnolipid-coated Pd-NZVI at total RL loading of 67 mg TOC/g NZVI). Insets represent total mass balances at end of reaction. Ethene and ethane were the reaction end-products. For all reactor systems studied, mass balance achieved was >90%.

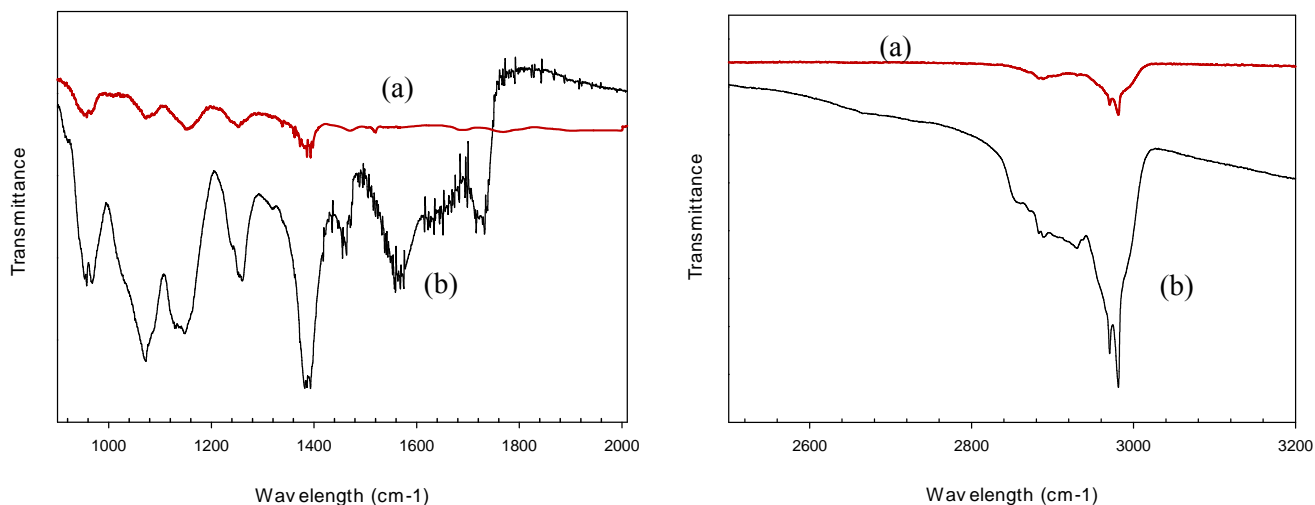


Figure S6: FTIR spectra of (a) RL-coated NZVI (b) RL

Figure S6 shows the FTIR spectrum of (a) RL coated NZVI and (b) RL.

RL spectra: The major peaks in the 3000-2800 cm^{-1} region are the $\nu_{\text{asym}}(\text{CH}_2)$ and $\nu_{\text{sym}}(\text{CH}_2)$ modes at 2960 and 2880 cm^{-1} , respectively. The low frequency region is dominated by the carboxylic acid $\nu_{\text{sym}}(\text{C}=\text{O})$ stretch at 1730 cm^{-1} and the $\nu_{\text{asym}}(\text{COO}^-)$ carboxylate mode at 1560 cm^{-1} . The region below 1500 cm^{-1} corresponds to the fingerprint region for rhamnolipid which includes vibrational modes of the rhamnose head group.^{8,9}

RL coated NZVI spectra: The asymmetric and symmetric CH_2 stretch did not show any change in the peak positions. However the $\nu_{\text{asym}}(\text{COO}^-)$ carboxylate mode shifted to 1520 cm^{-1} while the peak at $\nu_{\text{sym}}(\text{C}=\text{O})$ appeared to be split into a doublet. However the peak intensity isn't strong enough to conclude the splitting of the peak. However, overall it appears, that the interaction of rhamnolipid at the NZVI surface is through the carboxylate group.

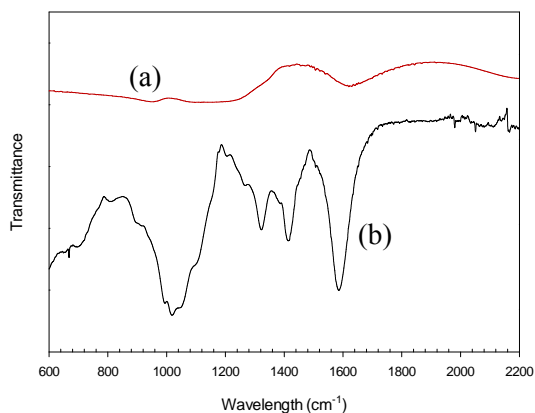


Figure S7: FTIR spectra of (a) CMC coated NZVI (b) CMC

Figure S7 shows the FTIR spectrum of (a) CMC coated NZVI and (b) CMC.

CMC spectra: The peaks observed at 1590 cm^{-1} and 1410 cm^{-1} are the $\nu_{\text{asym}}(\text{COO}^-)$ and $\nu_{\text{sym}}(\text{COO}^-)$ as well as the remaining peaks observed are in agreement with Cirtiu et. al¹.

CMC coated NZVI spectra: It was observed that the $\nu_{\text{asym}}(\text{COO}^-)$ carboxylate stretch shifted to 1610 cm^{-1} indicating CMC interacted with NZVI through the carboxylate group.

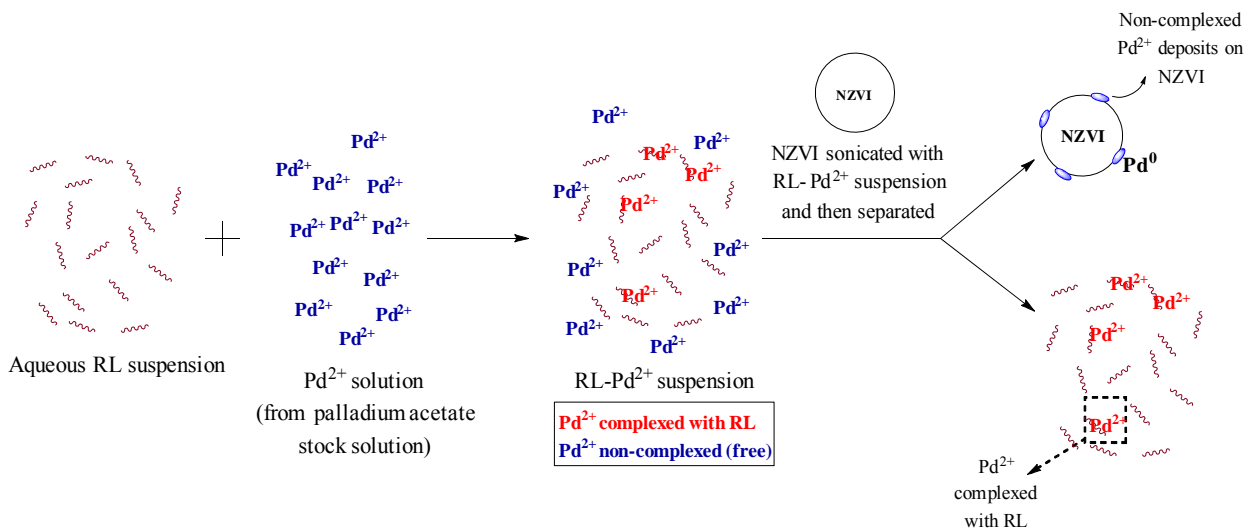


Figure S8: Schematic demonstrating the experimental design to quantify complexation by RL.

RL- Pd²⁺ Complexation:

In TCE degradation experiments, the system with total RL loading of 67 mg TOC/g NZVI, has

(a) RL in solution = 3 mg TOC/L, and

(b) RL adsorbed to NZVI surface = 40 mg TOC/g NZVI (Figure 4 in Manuscript).

PART I: First we quantified how much Pd²⁺ was complexed by 3 mg TOC/L RL.

We designed an experiment using uncoated NZVI as shown in Figure S8.

- (1) First, an aqueous suspension of 3 mg TOC/L RL was mixed with 0.75 mg/L Pd²⁺ (0.5% w/w of 150 mg/L NZVI) for 10 minutes.
- (2) Thereafter, the RL-Pd²⁺ suspension was sonicated with 150 mg/L NZVI for 15 minutes. Within a timeframe of 15 minutes, no RL sorbs to NZVI. Thus, in this step, the amount of Pd that deposits on NZVI can be attributed to Pd⁰ and it is derived from the free Pd²⁺ in the RL-Pd²⁺ suspension prior to contact with NZVI.
- (3) The supernatant was then decanted after centrifugation and retention of the NZVI with a super-magnet.
- (4) The separated NZVI (with Pd⁰ deposits on its surface) was then acid digested and analyzed in ICP-OES for quantification of Pd. This gives us the amount of non-complexed/free Pd²⁺ in the RL- Pd²⁺ suspension prior to contact with NZVI.
- (5) The supernatant was then acid digested and analyzed in ICP-OES to quantify the remainder of the Pd²⁺ (which did not deposit on NZVI in step 2) and was attributed to the amount of Pd²⁺ complexed with RL.

The mixing times between RL and Pd^{2+} was fixed based on their interaction time during synthesis of RL-coated Pd-NZVI in the TCE degradation experiments. No sorption of the of RL onto NZVI surface occurred during the 15 minute sonication time between NZVI and RL- Pd^{2+} suspension as confirmed through TOC analysis.

The experiment showed that, for a 0.03 mg nominal Pd dose,

- 0.009(± 0.001) mg Pd was complexed with 3 mg/L RL,
- while 0.021(± 0.001) mg Pd deposited on uncoated NZVI (which we attributed to non-complexed Pd^{2+}).

PART II: In the next step we compared the amount of Pd deposited on

- uncoated NZVI (measured in Part I) and
- the Pd deposited on NZVI coated with RL 40 mg TOC/g NZVI

Pd deposited on uncoated NZVI was 0.0021 mg (measured in part I).

We measured Pd deposited on the RL-coated NZVI to be 0.0078 mg.

Therefore the lower deposition on the RL-coated NZVI, is attributed to the lesser number of Pd deposition sites due to surface sorbed RL.

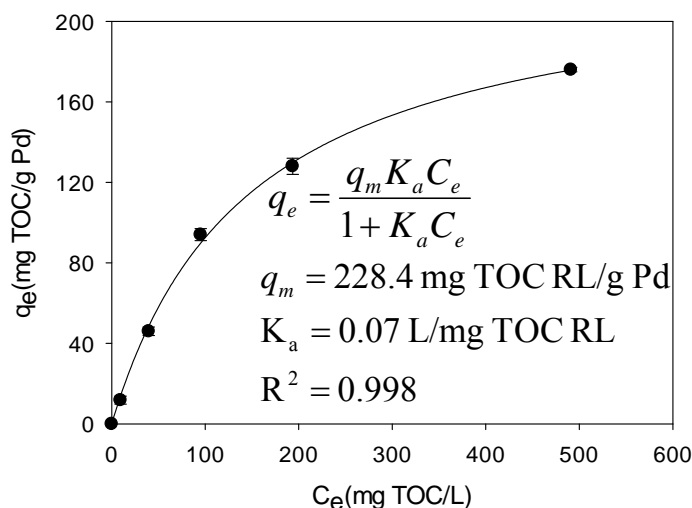
The amount of Pd^{2+} that did not deposit on RL-coated NZVI due to decrease in deposition sites, is 0.0132 mg Pd (0.021mg-0.0078mg)

Overall by combining PART I and PART II, we know:

Pd^{2+} complexed with 3 mg TOC/L RL = 0.009 mg

Pd^{2+} deposited on NZVI coated with RL 40 mg TOC/g NZVI = 0.0078 mg

Pd^{2+} undeposited = 0.0132 mg Pd



177

178 **Figure S9:** Sorption of RL to Pd⁰ nanoparticles fitted with Langmuir isotherm, where q_e is the
 179 equilibrium adsorption capacity of Pd⁰, C_e is the equilibrium aqueous phase concentration of RL, q_m is
 180 the maximum adsorption capacity of Pd⁰ and K_a is the adsorption equilibrium constant.

181 Pd⁰ nanoparticle synthesis: Palladium nanoparticles were synthesized using methods described
 182 previously^{10, 11} with certain modifications. 50 mg of Pd-acetate was added to 50 mL de-ionized water and
 183 sonicated for 5 minutes. The suspension turned yellowish-orange due to dissolution of Pd-acetate in
 184 water. 40 mL of the supernatant containing aqueous solution of Pd-acetate was then removed and mixed
 185 in a round-bottom flask using a magnetic stirrer for 15 minutes under N₂ flow. 10 mL of 1.5 g/L of
 186 sodium borohydride was then added drop-wise to the Pd-acetate solution which instantly turned black
 187 indicating the formation of Pd⁰ nanoparticles. The suspension was mixed for 1 hour. The concentration of
 188 Pd⁰ nanoparticles was determined using ICP-OES analysis and the nanoparticles were sized using
 189 Nanoparticle tracking analysis (NanoSight LM14). The mean size of nanoparticles obtained were 150±30
 190 nm. Stabilizing polymers to obtain highly monodisperse Pd⁰ or solvents such as ethanol to improve
 191 aqueous solubility of palladium acetate were not implemented in this synthesis because they interfere
 192 during the TOC analysis for determining the sorption isotherm as in Figure S9. The sorption isotherm was
 193 determined using similar procedures as described in the manuscript.

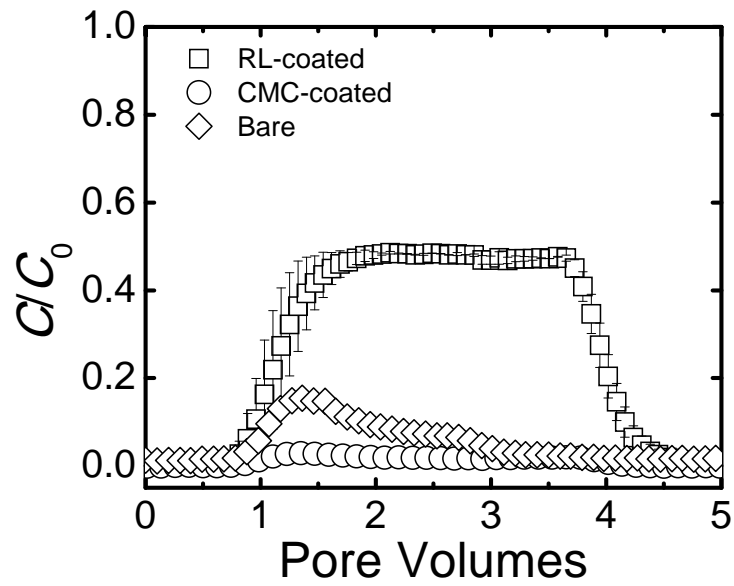


Figure S10: Measured breakthrough curves for rhamnolipid- and CMC- coated Pd-NZVI at 10 mM NaHCO_3 and pH 7.7. The surface modifier loading used was 13 mg TOC/g NZVI for both rhamnolipid and CMC. The transport experiments were conducted in a clean quartz sand column (mean grain size 651 μm and porosity 0.38) with an approach velocity of 7.5×10^{-5} m/s. (According to methods described in Basnet et al.¹²)

- 202 1. Cirtiu, C. M.; Raychoudhury, T.; Ghoshal, S.; Moores, A., Systematic comparison of the size,
203 surface characteristics and colloidal stability of zero valent iron nanoparticles pre-and post-grafted with
204 common polymers. *Colloids Surf. Physicochem. Eng. Aspects* **2011**, 390, (1), 95-104.
- 205 2. Mulligan, C. N., Environmental applications for biosurfactants. *Environmental pollution* **2005**,
206 133, (2), 183-198.
- 207 3. McIntyre, N.; Zetaruk, D., X-ray photoelectron spectroscopic studies of iron oxides. *Analytical*
208 *Chemistry* **1977**, 49, (11), 1521-1529.
- 209 4. Jeong, H. Y.; Han, Y.-S.; Park, S. W.; Hayes, K. F., Aerobic oxidation of mackinawite (FeS) and its
210 environmental implication for arsenic mobilization. *Geochimica et Cosmochimica Acta* **2010**, 74, (11),
211 3182-3198.
- 212 5. Basnet, M.; Di Tommaso, C.; Ghoshal, S.; Tufenkji, N., Reduced transport potential of a
213 palladium-doped zero valent iron nanoparticle in a water saturated loamy sand. *Water research* **2015**,
214 68, 354-363.
- 215 6. Burris, D. R.; Delcomyn, C. A.; Smith, M. H.; Roberts, A. L., Reductive dechlorination of
216 tetrachloroethylene and trichloroethylene catalyzed by vitamin B12 in homogeneous and
217 heterogeneous systems. *Environ. Sci. Technol.* **1996**, 30, (10), 3047-3052.
- 218 7. Rajajayavel, S. R. C.; Ghoshal, S., Enhanced reductive dechlorination of trichloroethylene by
219 sulfidated nanoscale zerovalent iron. *Water research* **2015**, 78, 144-153.
- 220 8. Lebron-Paler, A., *Solution and Interfacial Characterization of Rhamnolipid Biosurfactant from*
221 *Pseudomonas aeruginosa ATCC 9027*. ProQuest: 2008.
- 222 9. Leitermann, F.; Sylatk, C.; Hausmann, R., Fast quantitative determination of microbial
223 rhamnolipids from cultivation broths by ATR-FTIR Spectroscopy. *Journal of biological engineering* **2008**,
224 2, (1), 1-8.
- 225 10. NaiduáKona, C., A simple method for the preparation of ultra-small palladium nanoparticles and
226 their utilization for the hydrogenation of terminal alkyne groups to alkanes. *Nanoscale* **2015**, 7, (3), 872-
227 876.
- 228 11. Ugalde-Saldivar, V., Aerobic synthesis of palladium nanoparticles. *Rev. Adv. Mater. Sci* **2011**, 27,
229 31-42.
- 230 12. Basnet, M.; Ghoshal, S.; Tufenkji, N., Rhamnolipid biosurfactant and soy protein act as effective
231 stabilizers in the aggregation and transport of palladium-doped zerovalent iron nanoparticles in
232 saturated porous media. *Environ. Sci. Technol.* **2013**, 47, (23), 13355-13364.